At-wavelength figure metrology of total reflection mirrors in hard x-ray region

Yumoto, Hirokatsu, Mimura, Hidekazu, Matsuyama, Satoshi, Handa, Soichiro, Shibatani, Akihiko, et al.

Hirokatsu Yumoto, Hidekazu Mimura, Satoshi Matsuyama, Soichiro Handa, Akihiko Shibatani, Keiko Katagishi, Yasuhisa Sano, Makina Yabashi, Yoshinori Nishino, Kenji Tamasaku, Tetsuya Ishikawa, Kazuto Yamauchi, "At-wavelength figure metrology of total reflection mirrors in hard x-ray region," Proc. SPIE 6317, Advances in X-Ray/EUV Optics, Components, and Applications, 631709 (29 August 2006); doi: 10.1117/12.681587

SPIE.

Event: SPIE Optics + Photonics, 2006, San Diego, California, United States

Invited Paper

At-wavelength figure metrology of total reflection mirrors in hard x-ray region

Hirokatsu Yumoto*[a], Hidekazu Mimura[a], Satoshi Matsuyama[a], Soichiro Handa[a], Akihiko Shibatani[a], Keiko Katagishi[a], Yasuhisa Sano[a], Makina Yabashi[b], Yoshinori Nishino[c], Kenji Tamasaku[c], Tetsuya Ishikawa[b,c], and Kazuto Yamauchi[a]
[a]Graduate School of Engineering, Osaka University, 2-1 Yamada-oka, Suita, Osaka 565-0871, Japan
[b]SPring-8/Japan Synchrotron Radiation Research Institute (JASRI), 1-1-1, Kouto, Sayo-cho, Sayo-gun, Hyogo 679-5198, Japan
[c]SPring-8/RIKEN, 1-1-1, Kouto, Sayo-cho, Sayo-gun, Hyogo 679-5198, Japan

ABSTRACT

We realized nearly diffraction-limited performance with a FWHM focal spot size of 25 nm at an x-ray energy of 15 keV at SPring-8. We explain performances of fabricated x-ray mirror, its fabrication technologies and future plan for realizing sub-10-nm focusing. We developed a novel method of at-wavelength metrology for evaluating the focusing hard x-ray beam in a grazing-incidence optical system. The metrology is based on the numerical retrieval method using the intensity distribution profile around the focal point. We demonstrated the at-wavelength metrology and estimated the surface figure error on a test mirror. An experiment for measuring the focusing intensity profile was performed at the 1-km-long beamline (BL29XUL) of SPring-8. The obtained results were compared with the profile measured by the optical interferometer and confirmed to be in good agreement with it. This technique has potential for characterizing wave-front aberration on elliptical mirrors for the sub-10-nm focusing.

Keywords: hard X-ray mirror, X-ray nanofocusing, at-wavelength wave-front metrology, surface figure metrology, and fabrication technique

1. INTRODUCTION

Progress in the fields of science is supported by precision technologies. In recent years, a combination of third-generation synchrotron radiations and optical elements, which are manufactured through technological means, has enabled the realization of hard x-ray nanobeams with lateral beam sizes less than 100 nm. Hard x-ray nanobeams are applied to scanning hard x-ray microscopy, microdiffraction analysis, and spectromicroscopy in analyses in medicine, chemistry, materials science, and other science fields. These techniques have the ability to analyze materials nondestructively with precise spatial information. The spatial and contrast resolutions of these microscopes are determined not only by the focusing size of the hard x-ray beam, but also by the intensity distribution properties of the focused beam. An ideally focused beam, the so-called diffraction-limited focused beam, allows one to obtain an excellent resolution of the microscope used. There are many types of hard x-ray focusing optics, which use refraction, reflection, and diffraction effects, such as Fresnel Zone plates, Kirkpatrick-Baez (K-B) mirrors, compound refractive lenses, Bragg-Fresnel lenses, and capillaries. The focusing probes generated using K-B mirrors, which utilize two concave mirrors at a glancing angle to collect and focus x-rays in both vertical and horizontal axes, have a high efficiency in comparison with other optics. A doubly focused full width at half maximum (FWHM) 36×48 nm^2 nearly diffraction-limited beam at 15 keV was obtained using K-B mirrors in our previous research of Mimura *et al.*[1].

The quality of the focusing probes obtained by K-B mirrors is influenced by optical design, surface figure accuracy, degree of coherence of illumination light, and alignment accuracy. We have developed the manufacturing process of

*yumoto@up.prec.eng.osaka-u.ac.jp; phone +81-6-6879-7286; fax +81-6-6879-7286

Advances in X-Ray/EUV Optics, Components, and Applications, edited by Ali M. Khounsary and Christian Morawe,
Proc. of SPIE Vol. 6317, 631709, (2006) · 0277-786X/06/$15 · doi: 10.1117/12.681587

directly figured elliptical mirrors for diffraction-limited focusing in hard x-rays and applied them to a scanning x-ray microscope [2]-[4]. Computer-controlled plasma chemical vaporization machining (PCVM) [5] and elastic emission machining (EEM) [6] can figure mirror surfaces to a peak-to-valley (PV) accuracy better than 1 nm and lateral resolutions close to 0.1 mm [1],[7],[8]. In addition, surface figure metrology combining microstitching interferometry (MSI) [9] with relative angle determinable stitching interferometry (RADSI) [10] can measure the surface profiles of an x-ray mirror to a PV accuracy better than 3 nm and a spatial resolution close to 10 μm.

One of the most important matters regarding hard x-ray focusing is the improvement of the focusing beam size. To realize a smaller focusing size, mirrors with steeply curve having a larger numerical aperture (NA) are necessary. In this study, we designed two types of mirrors. One is a total-reflection mirror and the other is a multilayer mirror. First, we explain a total-reflection line-focusing mirror, which we fabricated, having a designed focal size of 22 nm at an x-ray energy of 15 keV. Line-focusing test was performed at 1-km-long beam line (BL29XUL) of SPring-8 [11]. Nearly diffraction-limited performance with a FWHM focal spot size of 25 nm at an x-ray energy of 15 keV was realized. Second, we explain a multilayer mirror for focusing hard x-rays to a sub-10-nm size. As we will describe, we examined the acceptable tolerance of wave-front error to realize diffraction-limited sub-10-nm focusing. The wave-front aberration tolerance places extremely high demands on the fabrication of mirror substrates and multilayer coatings, and even higher demands on the metrology tools required to evaluate mirror surface qualities. Conventional surface metrologies are not sufficient. In the extreme ultraviolet (EUV) wavelength region, wave-front metrology is an essential tool for the development of diffraction-limited optical systems for lithography [12]. The system performance, composed of the geometric figure of the substrate surface and the properties of the multilayer coatings, is measurable only at the operational wavelength.

In this article, we suggest a new method of at-wavelength metrology for evaluating diffraction-limited focusing mirrors in the hard x-ray region [13]. At-wavelength metrology for estimating the wave-front aberration of reflected x-rays is based on numerical calculation using the intensity distribution around the focal point.

We demonstrated the at-wavelength metrology for a total-reflection mirror at 15 keV. The calculated profile was in good agreement with that measured by MSI, which indicates the effectiveness of the developed method.

2. FABRICATION OF TOTAL-REFLECTION MIRROR

2.1 Design of Total-Reflection Mirror

Table 1 lists the optical parameters of this system. The designed surface is a partial profile of an elliptic function in which one focal point is the position of an incident slit as an x-ray source and the other is the position where x-rays collect. The mirror was designed for the 1-km-long beamline (BL29XUL) of SPring-8. The focal length is set to be 50 mm. Figure 1 shows the designed elliptical profile. Figure 2 shows the predicted intensity profile at the focal plane at 15 keV, which is obtained by a wave-optical simulator coded on the basis of the Fresnel-Kirchhoff diffraction integral theory [2]. The relationship between figure error characteristics and focusing property has been investigated using a wave-optical simulator. The obtained results indicate that the figure errors characterized in the middle spatial wavelength range affects the shape of the focused beam profile and the figure errors characterized in the short spatial wavelength range decreases the efficiency. To realize the ideal beam focal size, the figure accuracy needs to be at least 4 nm PV in the middle spatial wavelength range.

Table. 1. Optical parameters of designed total- reflection mirror

Mirror length	50 mm
Lengh of ellipse	500.025 m
Breadth of ellipse	20.79 mm
Focal length	50 mm
Glancing angle on optical axis	2.94 mrad
Acceptance width	0.13 mm
Surface coating	Pt

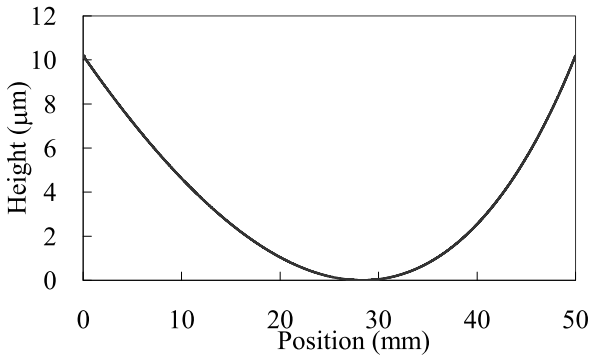

Fig. 1. Surface figure profile of designed total- reflection mirror substrate.

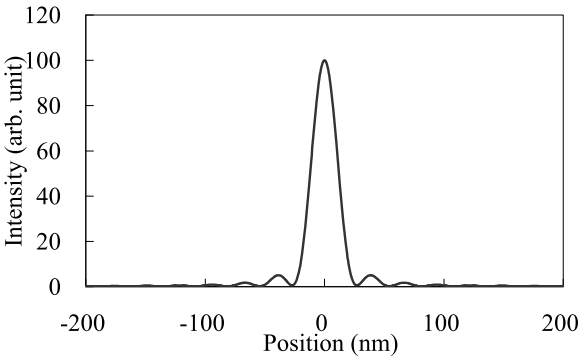

Fig. 2. Intensity profile of ideally focused x-ray beam at 15 keV, which is calculated using wave-optical simulator.

2.2 Manufacturing Process of Total-Reflection Mirror

The x-ray mirror was fabricated by figuring substrate surface shape into a designed one with required accuracy for ideal focusing, using a computer-controlled fabrication system consist of plasma chemical vaporization machining (PCVM) and elastic emission machining (EEM). Then platinum was coated on the figured surface area using a scanning-type platinum deposition system. Microstitching interferometry (MSI) and relative angle determinable stitching interferometry (RADSI) were developed for testing the surface profiles. By combining both MSI with RADSI, the surface figure can be measured with a PV accuracy better than 3 nm and a spatial resolution close to 10 μm.

2.3 Line-Focusing Test of Total-Reflection Mirror

The line-focusing test was performed at the 1-km-long beamline (BL29XUL) of SPring-8 because the available incident x-ray had been confirmed to have sufficient coherence to evaluate ultraprecise mirrors. Wire scanning method was employed for detecting the focusing intensity distribution profile. A piezoactuated translation stage enabled wire scanning at a 5 nm increments. A gold wire having a diameter of 200 μm was used. Figure 3 shows the intensity profile measured under the best focusing condition and shows the simulated beam profile obtained by calculating the Fresnel-Kirchhoff integral using the measured mirror surface figure as the boundary condition. The measured profile has completely raw data without any compensation taking the transmission effect at the gold wire edge into account. Nearly diffraction-limited performance with a FWHM focal spot size of as narrow as 25 nm was realized at an x-ray energy of 15 keV. The fairly good agreement between the measured and calculated profiles indicates the effectiveness of metrology in fabricating the mirror and of predicting focusing performance.

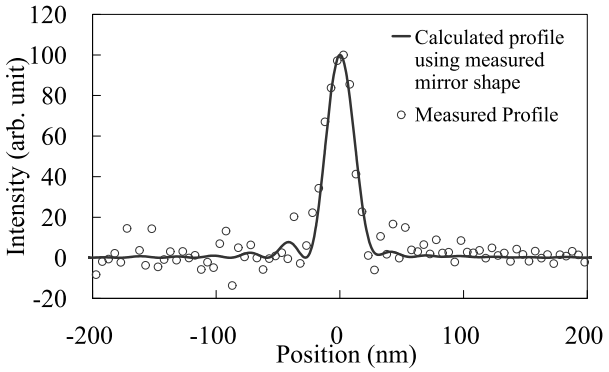

Fig. 3. Intensity profile measured under best focusing conditions, and calculated intensity profile using measured mirror shape. X-ray energy is 15 keV.

3. OPTICAL DESIGN FOR SUB-10-NM FOCUSING

3.1 Design of optical parameter

We designed the line-focusing mirror with a large NA having a 1.1 mm aperture size and a 100 mm long working distance assuming application of this mirror in a microscope system. Table 2 lists the optical parameters of the sub-10-nm focusing system. Figure 4 shows the figure profile of the designed 100-mm-long mirror substrate. The surface shape of the mirror is part of an elliptical function in which one focal point is the light source and the other is the focal point. The mirror was designed for the 1- km-long beamline of SPring-8 [11] where the mirror aperture can be coherently illuminated. The incidence angle on the optical axis is 11.1 mrad. By coating graded multilayers [14], which fulfill the Bragg diffraction condition, a high reflectivity can be maintained at an incidence angle larger than the critical angle of the substrate material. Figure 5 shows the predicted intensity profile at a focal plane at an x-ray energy of 15 keV, which is obtained using a wave-optical simulator [2],[15] coded on the basis of the Fresnel-Kirchhoff diffraction integral theory. The ideal focusing size is 9.2 nm (FWHM).

Table. 2. Optical parameters of designed multilayer mirror

Mirror length	100 mm
Lengh of ellipse	500.075 m
Breadth of ellipse	135.9 mm
Focal length	150 mm
Glancing angle on optical axis	11.1 mrad
Acceptance width	1.1 mm
Surface coating	Graded Pt/C multilayer
Number of multilayer periods	20
Reflectivity in the first order on optical axis	60 %
Double layer spacing (d spacing) on optical axis	3.7 nm

3.2 Acceptable tolerance of wave-front error

We examined the acceptable tolerance of wave-front error to realize the diffraction-limited sub-10-nm focusing in this optical system. A wave-front accuracy of 1/4 λ (λ is the wavelength) is required in accordance with Rayleigh's quarter wavelength rule [16]. The wave-front error φ, attributed to the figure error height d, is expressed by the following equation in grazing-incidence total-reflection mirror optics.

$$\varphi = 2\, d\, k \sin\theta. \quad (1)$$

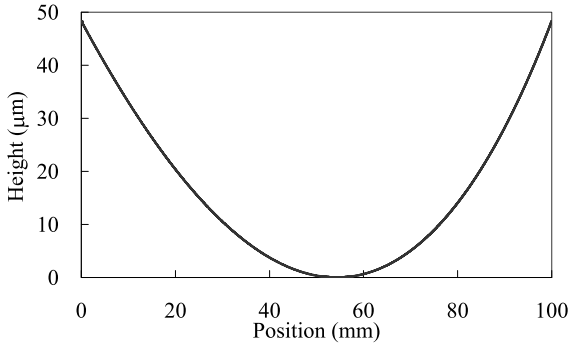

Fig. 4. Surface figure profile of designed mirror for nanofocusing of hard x-rays.

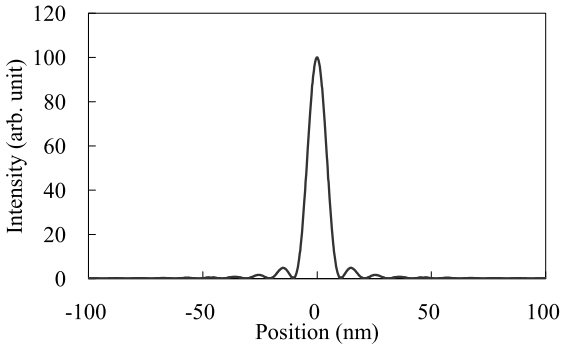

Fig. 5. Intensity profile of ideally focused x-ray beam at 15 keV, which is calculated using wave-optical simulator.

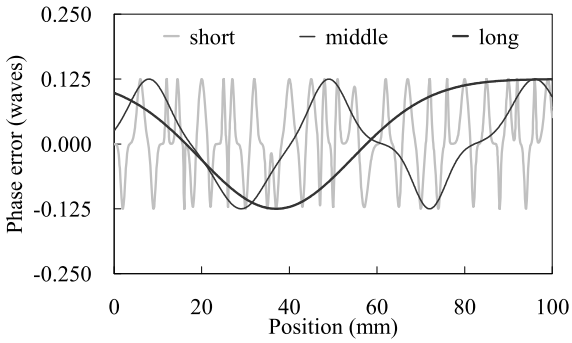

Fig. 6. Phase error profiles characterized in short, middle, and long spatial wavelength ranges used in simulation for estimating wave-front aberration tolerance. PV phase error height corresponds to 1/4 λ.

Here, θ is the glancing angle of an incident beam at the reflecting point, and k is the wave number. Wave-front error corresponds to the figure error in this optical system. The mutual relationships between the phase error characteristics and the focusing performances were investigated using the wave-optical simulator. Figure 6 shows the phase error profiles characterized in short, middle, and long spatial wavelength ranges in the longitudinal direction of the mirror. The PV phase error height is 1/4 λ, which is equal to a figure error height of 0.93 nm at the optical axis of this mirror. Figure 7 shows the calculated intensity profiles of focused x-ray beams using the elliptical mirror having the phase errors shown

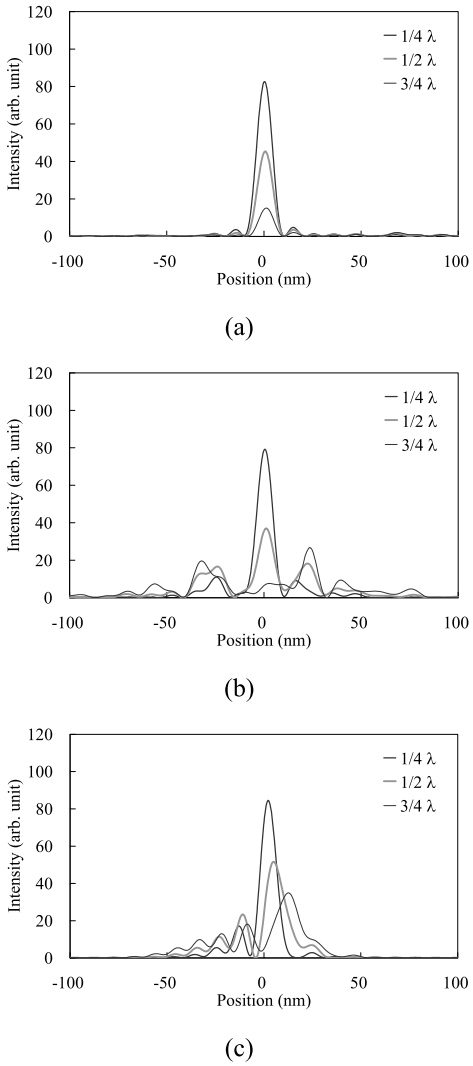

Fig. 7. Calculated intensity distribution profiles at focal plane using designed mirror having phase error height PV 1/4 λ, 1/2 λ, and 3/4 λ at an x-ray energy of 15 keV. (a)Short, (b)Middle, and (c)Long spatial wavelength ranges.

in Fig. 6. This simulation results indicate that the phase errors in the middle spatial wavelength range deform the shapes of the focal beam profiles and that the phase errors in the short spatial wavelength range decrease the intensity of the focused beam. From these results, a PV figure error height of lower than 0.93 nm, corresponding to a phase error of 1/4 λ accuracy, is necessary for the metrology to realize the diffraction-limited focusing beam. Using the optical interferometer, the short spatial wavelength range is measurable with a 0.1 nm height accuracy. Metrology in the middle spatial wavelength range is desired.

4. AT-WAVELENGTH METROLOGY

We developed a method of evaluating the phase error of the focusing wave-front x-ray due to the imperfections of the mirror. The observable physical value is the reflected intensity distribution from the test mirror without its phase information. Reconstructing the phase only from the intensity information is referred to as a phase problem. A Fourier-based iterative algorithm [17]-[19] and other algorithms [20],[21] have been used to perform such a reconstruction. We developed two types of phase-retrieval algorithm in this study. One is based on an iterative-transform algorithm and the

other is based on linear-optimization algorithms. In both retrieval programs, we applied the designed optical arrangement in our previously developed wave-optical simulator [2] to investigate the intensity distribution reflected by the mirror. Furthermore, we assumed a transverse coherence length of infinity at the light source in the model, because this enabled significant simplification of the algorithm. In the designed optical system, x-rays illuminating the mirror are produced at an undulator and propagate for a long distance of 1 km. This designed optical system provides perfect coherent illumination on the mirror. The propagation of wave field $\Psi_0(r_0)$ on an s_0 screen at r_0 to $\Psi_1(r_1)$ on an s_1 screen is obtained as follows from the Fresnel-Kirchhoff diffraction formula [22]:

$$\Psi_1(r_1) = I_1(r_1)\cdot\exp(i\phi_1(r_1)) \tag{2}$$

$$= -\frac{i}{2\lambda}\int_{s_0}\Psi_0(r_0)\frac{\exp(ikr_{01})}{r_{01}}(1+\cos\chi)ds\,, \tag{3}$$

where $I_1(r_1) = |\Psi_1(r_1)|$ is the magnitude of the complex wave field, $\phi_1(r_1)$ is the phase of the wave field, $r_{01}=r_1-r_0$, and $-\frac{i}{2\lambda}(1+\cos\chi)$ is the inclination factor [22]. A wave field at focal plane Ψ_f is calculated using a wave field Ψ_m on the mirror surface. Ψ_m is calculated using a wave field Ψ_s on an incident slit.

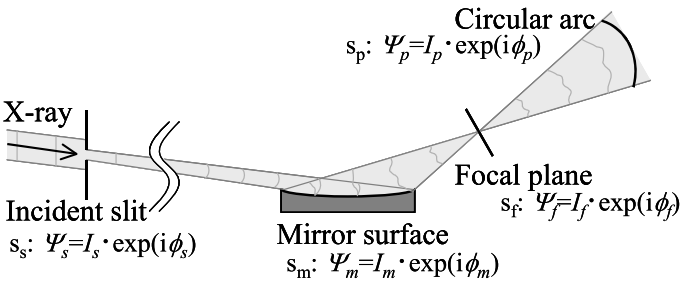

Fig. 8. Schematic layout of optical system for phase retrieval.

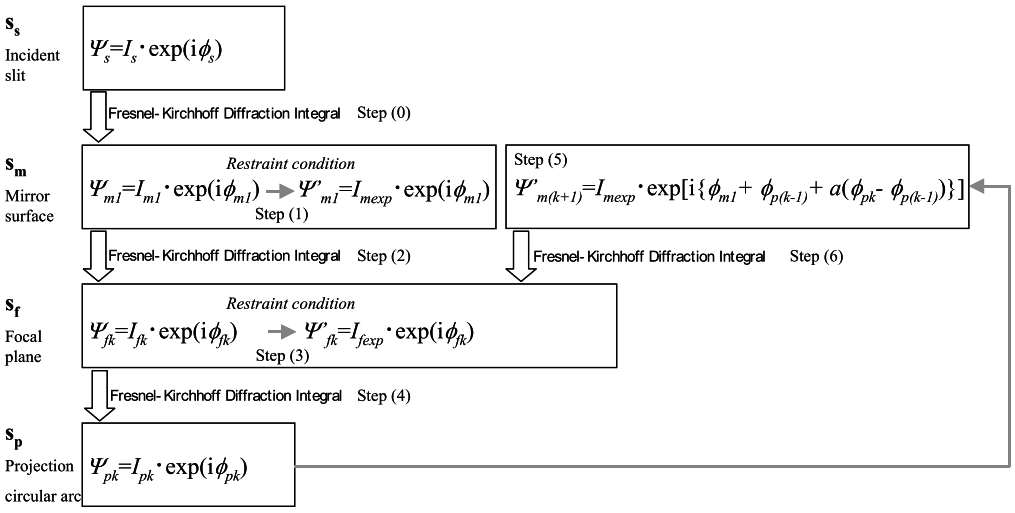

Fig. 9. Block diagram of phase retrieval algorithm.

4.1 Iterative-transform method

The wave-front error of the focusing beam is calculated on the basis of an error-reduction algorithm [23]. The mirror is assumed to shift the phase of the reflected wave and change the known intensity, because of its imperfections. The mirror acts as a pure phase object in the developed phase retrieval program. Wave-front error calculation is performed from a single intensity distribution. We define a projection circular arc s_p. Figure 8 shows a schematic of the optical system for the phase retrieval. The phase retrieval problem is the recovery of phase ϕ_p on an s_p, which is equivalent to the wave-front phase error of the focusing beam, from the observed intensities I_{fexp}^2 of the focal plane and I_{mexp}^2 on the mirror surface. Figure 9 is a block diagram showing the phase retrieval algorithm. The phase retrieval algorithm consists of the following steps:

(0) Propagate through incident slit $s_s \rightarrow$ the mirror surface s_m : $\Psi_{m1}=I_{m1}\cdot\exp(i\phi_{m1})$. In this case, $\Psi_s=1$ is defined. The perfectly elliptical shape of the surface is taken as the initial point of the iteration algorithm because the surface shape of the mirror can be measured approximately using the optical interferometer.

(1) The magnitude of Ψ_{m1} is replaced with the measured modulus I_{mexp}.

(2) Propagate s_m : $\Psi'_{m1}= I_{mexp}\cdot\exp(i\phi_{m1}) \rightarrow$ the focal plane s_f : $\Psi_{fk}=I_{fk}\cdot\exp(i\phi_{fk})$. k=1

(3) The magnitude of Ψ_{fk} is replaced with the measured modulus I_{fexp} at the kth iteration.

(4) Propagate s_f : $\Psi'_{fk}= I_{fexp}\cdot\exp(i\phi_{fk}) \rightarrow s_p$: $\Psi_{pk}=I_{pk}\cdot\exp(i\phi_{pk})$.

(5) The phase of $\Psi_{m(k+1)}$ is replaced with $\{\phi_{m1}+\phi_{p(k-1)}+\alpha(\phi_{pk}-\phi_{p(k-1)})\}$. α, the step size, is a positive constant. ($\phi_{p(k-1)}$=0 at k=1.)

(6) Propagate s_m : $\Psi'_{m(k+1)}=I_{mexp}\cdot\exp[i\{\phi_{m1}+\phi_{p(k-1)}+\alpha(\phi_{pk}-\phi_{p(k-1)})\}] \rightarrow s_f$: $\Psi_{f(k+1)}=I_{f(k+1)}\cdot\exp(i\phi_{f(k+1)})$.

Then, steps (3)-(6) are repeated to obtain a consistent ϕ_p. In step (4), the wave-front error on the mirror surface is calculated. We assume the wave-front of the focusing wave to be of the same form and independent of the distance from the focal point if the distance is sufficiently large, because the wave-front error under consideration is sufficiently small.

Simulation was performed to explore the characteristics of the phase retrieval algorithm. The simulated optical system is designed to achieve sub-10-nm focusing, and the assumed phase error on the mirror surface is shown in Figure 11 (a). Figure 10 shows the focusing intensity profiles recovered (b) and set as the original value (a). Figure 11 (b) shows the recovered phase error on the ideal surface curve. Approximately 1000 iterations were performed to obtain the result. From the intensity profile, including no measurement noise, an accuracy on the order of 0.030 waves root-mean-square (RMS) was simulated under these conditions.

The Fourier transform of the complex amplitude distribution of the focusing light wave becomes a complex amplitude distribution at the focal plane. From this viewpoint, the intensity distribution around the focal point is more sensitive to the middle and long spatial wavelength ranges than to the short range. This wave-front metrology has a higher potential for evaluating focusing optics than an optical interferometer.

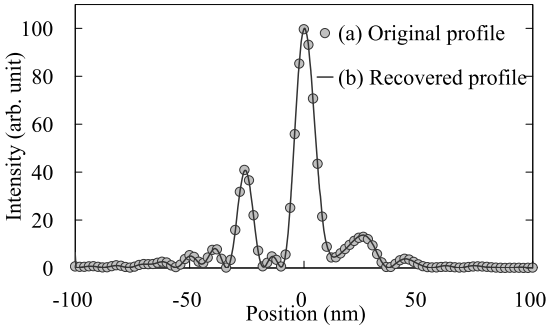

Fig. 10. Results of numerical simulation of phase retrieval algorithm. Intensity distribution profiles at focal point. (a) Original intensity profile. (b) Reconstructed intensity profile.

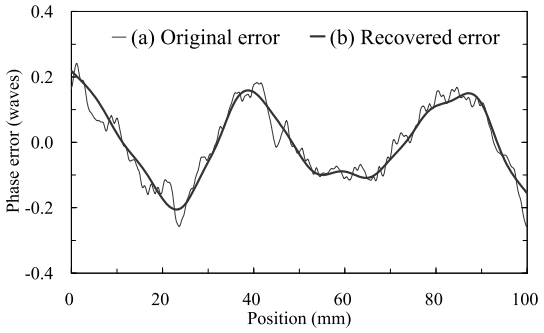

Fig. 11. Results of numerical simulation of phase retrieval algorithm. Phase error distribution on ideally shaped mirror surface. (a) Original phase error. (b) Phase error distribution reconstructed from intensity at focal point.

4.2 Linear-optimization method

The other approach to determining wave-front error is the iteration method, which minimizes the differential intensity between experimental and simulated data by solving a direct problem [2]. A wave-front error is expressed as a weighting function of unit phase error. The error parameters are composed of PV height and spatial wavelength in the longitudinal direction of the mirror. This method allows us to find the solution even if the measured intensities contain noise. One of the main problems of this phase retrieval method is the long computation time. To overcome this difficulty, the coded program is substantially simplified. The iterative procedure is continued until no further improvement is observed.

To avoid the local minimum problem, the two developed algorithms are combined to calculate wave-front error using the measured intensity distribution. Additional intensity measurements around the focal point are of assistance in performing high-precision computation.

4.3 Experiment

At-wavelength wave-front metrology for a total reflection mirror at 15 keV was demonstrated. The experiment was performed using the 1-km-long beamline (BL29XUL) of SPring-8. The test mirror has a much smaller NA than the designed sub-10-nm focusing mirror. The test mirror surface can be measured with a high accuracy by MSI and a focusing intensity profile of 200 nm (FWHM) can be detected accurately by a wire scanning method. The optical parameters of this mirror are shown in Table 3. Figure 12 shows (a), (b) the measured intensity profiles, and (c) the recovered intensity profile using the retrieval algorithm at the focusing point. The intensity profiles were measured at 25 nm and 50 nm intervals independently. Figure 13 shows the phase error profiles on the test mirror surface (a) measured by MSI and (b) recovered using the retrieval algorithm. In this optical system, the phase error of 1/4 λ corresponds to a figure error height of 7.4 nm at the mirror center. Although the retrieval accuracy depends on the precision of the intensity measurement of the focusing beam, the difference in wave-front error between the two phase errors is 0.052 waves RMS. The good agreement between the two figure error profiles in the middle spatial wavelength range proves the high capability of the developed metrology, not shared by conventional surface metrologies, to realize diffraction-limited focusing.

Table. 3. Optical parameters of test mirror.

Substrate material	CZ-Si (111) single crystal
Surface coating	None
Effective mirror length in longitudinal direction	90 mm
Lengh of ellipse	500.15 m
Breadth of ellipse	24.25mm
Focal length	300mm
Glancing angle on optical axis	1.40 mrad
Acceptance width	130 μm

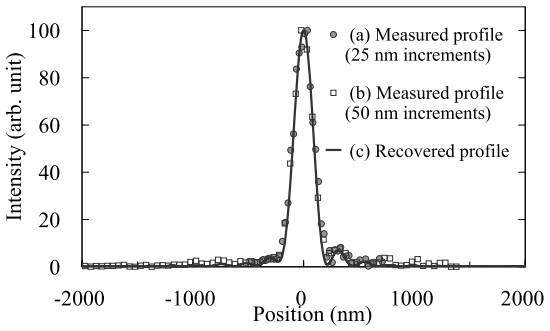

Fig. 12. Experimental results of at-wavelength metrology. Intensity distribution profiles at focal point at an x-ray energy of 15 keV. (a), (b) Measured intensity profile using wire-scanning method. (a) Circles denote 25 nm increments and (b) Squares denote 50 nm increments. (c) Reconstructed intensity profile using phase retrieval algorithm.

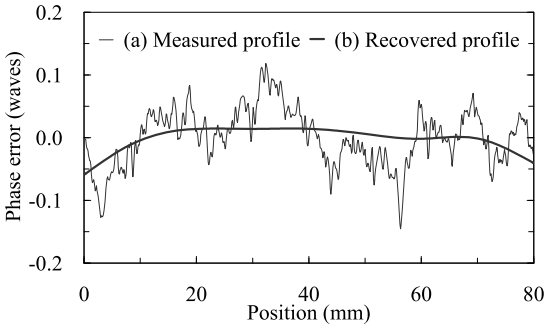

Fig. 13. Experimental results of at-wavelength metrology. Phase error distribution on ideal shape plane of focusing mirror. (a) Measured profile using optical interferometer. (b) Reconstructed profile from measured intensity profile at focal point.

5. RESULTS

Nearly diffraction-limited performance with a FWHM spot size of 25 nm was realized at 15 keV. We showed the future plan for realizing sub-10-nm focusing. We have developed and demonstrated efficient at-wavelength wave-front metrology. Realization of the sub-10-nm diffraction-limited focusing requires a manufacturing process consisting of the at-wavelength assessment of the fabricated mirror and the phase correction of wave-front aberration on the basis of the estimated phase error. Therefore, the at-wavelength wave-front metrology presented here is an indispensable tool. One of the technical considerations of the process is the accuracy of the characterizing method for the sub-10-nm focusing intensity distribution. Several techniques have been used to evaluate the nanobeams [24]-[29], however, these have not been demonstrated in the sub-10-nm region.

At-wavelength wave-front metrology is also applicable to microdiffraction, in which the illuminated x-ray wave front over the object must be known. Sub-10-nm hard x-ray probes with extremely intense light will revolutionize the field of microscopy. This technique offers the ability to realize nondestructive analyses of the internal structure of materials with the same spatial resolution as electron microscopy and AFM (atomic force microscopy), and moreover, to realize monomolecular resolution analyses.

ACKNOWLEDGMENTS

This research was supported by Grant-in-Aid for Specially Promoted Research 18002009, 2006 and 21st Century COE Research, Center for Atomistic Fabrication Technology, 2006 from the Ministry of Education, Sports, Culture, Science and Technology, Japan.

REFERENCES

1. H. Mimura *et al.*, “Hard X-ray Diffraction-Limited Nanofocusing with Kirkpatrick-Baez Mirrors.” Jpn. J. Appl. Phys. **44**, 539-542, (2005).
2. S. Matsuyama *et al.*, “Diffraction-limited two-dimensional hard-x-ray focusing at the 100 nm level using a Kirkpatrick-Baez mirror arrangement.” Rev. Sci. Instrum. **76**, 083114, (2005).
3. H. Yumoto *et al.*, “Fabrication of elliptically figured mirror for focusing hard x rays to size less than 50 nm.” Rev. Sci. Instrum. **76**, 063708, (2005).
4. S. Matsuyama, *et al.*, "Hard x-ray nano-focusing at 40nm level using K-B mirror optics for nanoscopy/spectroscopy" Proc. SPIE **5918** 591804 (2005).
5. K. Yamamura *et al.*, “Fabrication of elliptical mirror at nanometer-level accuracy for hard x-ray focusing by numerically controlled plasma chemical vaporization machining.” Rev. Sci. Instrum. **74**, 4549-4553, (2003).
6. K. Yamauchi, H. Mimura, K. Inagaki, and Y. Mori, “Figuring with subnanometer-level accuracy by numerically controlled elastic emission machining.” Rev. Sci. Instrum. **73**, 4028-4033, (2002).
7. H. Mimura *et al.*, “Image quality improvement in a hard X-ray projection microscope using total reflection mirror optics.” J. Synchrotron Radiat. **11**, 343-346, (2004).
8. K. Yamauchi *et al.*, “Two-dimensional Submicron Focusing of Hard X-rays by Two Elliptical Mirrors Fabricated by Plasma Chemical Vaporization Machining and Elastic Emission Machining.” Jpn. J. Appl. Phys., Part 1 **42**, 7129-7134, (2003).
9. K. Yamauchi *et al.*, “Microstitching interferometry for x-ray reflective optics.” Rev. Sci. Instrum. **74**, 2894-2898 (2003).
10. H. Mimura *et al.*, “Relative angle determinable stitching interferometry for hard x-ray reflective optics.” Rev. Sci. Instrum. **76**, 045102 (2005).
11. K. Tamasaku, Y. Tanaka, M. Yabashi, H. Yamazaki, N. Kawamura, M. Suzuki, and T. Ishikawa, “SPring-8 RIKEN beamline III for coherent X-ray optics.” Nucl. Instrum. Methods Phys. Res. A **467–468**, 686–689, (2001).
12. H. Medecki, E. Tejnil, K. A. Goldberg, and J. Bokor, “Phase-shifting point diffraction interferometer.” Opt. Lett. **21**, 1526-1528 (1996).
13. H. Yumoto, H. Mimura, S. Matsuyama, S. Handa, Y. Sano, M. Yabashi, Y. Nishino, K. Tamasaku, T. Ishikawa, and K. Yamauchi, “At-wavelength figure metrology of hard x-ray focusing mirrors.” Rev. Sci. Instrum. **77**, 063712, (2006).
14. Ch. Morawe, P. Pecci, J. Ch. Peffen, and E. Ziegler, “Design and performance of graded multilayers as focusing elements for x-ray optics.” Rev. Sci. Instrum. **70**, 3227-3232 (1999).
15. K. Yamauchi et al., “Wave-optical evaluation of interference fringes and wavefront phase in a hard-x-ray beam totally reflected by mirror optics.” Appl. Opt. **44**, 6927-6932, (2005).
16. M. Born and E. Wolf, Principles of Optics, 6th ed. (Cambridge University Press, 1997), p. 468.
17. J. Miao, P. Charalambous, J. Kirz, and D. Sayre, “Extending the methodology of X-ray crystallography to allow imaging of micrometre-sized non-crystalline specimens.” Nature (London) **400**, 342-344 (1999).
18. Y. Nishino, J. Miao, and T. Ishikawa, “Image reconstruction of nanostructured nonperiodic objects only from oversampled hard x-ray diffraction intensities.” Phys. Rev. B **68**, 220101, (2003).
19. H. M. Quiney, A. G. Peele, Z. Cai, D. Paterson, and K. A. Nugent, “Diffractive imaging of highly focused X-ray fields.” Nature Physics **2**,101-104 (2006).
20. A. Souvorov, M. Yabashi, K. Tamasaku, T. Ishikawa, Y. Mori, K. Yamauchi, K. Yamamura, and A. Saito, “Deterministic retrieval of surface waviness by means of topography with coherent X-rays.” J. Synchrotron Radiat. **9**, 223-228, (2002).
21. J. R. Fienup, “Phase-retrieval algorithms for a complicated optical system.” Appl. Opt. **32**, 1737-1746, (1993).
22. M. Born and E. Wolf, Principles of Optics, 7th ed. (Cambridge University Press, 2001), p. 422-423.
23. J. R. Fienup, “Phase retrieval algorithms: a comparison.” Appl. Opt. **21**, 2758-2769 (1982).

24. Y. Suzuki, A. Takeuchi, H. Takano, and H. Takenaka, “Performance Test of Fresnel Zone Plate with 50 nm Outermost Zone Width in Hard X-ray Region.” Jpn. J. Appl. Phys. **44**, 1994-1998, (2005).
25. W. Liu, G. E. Ice, J. Z. Tischler, A. Khounsary, C. Liu, L. Assoufid, and A. T. Macrander, “Short focal length Kirkpatrick-Baez mirrors for a hard x-ray nanoprobe.” Rev. Sci. Instrum. **76**, 113701 (2005).
26. O. Hignette, P. Cloetens, G. Rostaing, P. Bernard, and C. Morawe, “Efficient sub 100 nm focusing of hard x rays.” Rev. Sci. Instrum. **76**, 063709, (2005).
27. C. G. Schroer *et al.*, “Hard x-ray nanoprobe based on refractive x-ray lenses.” Appl. Phys. Lett. **87**, 124103, (2005).
28. H. C. Kang, J. Maser, G. B. Stephenson, C. Liu, R. Conley, A. T. Macrander, and S. Vogt, “Nanometer Linear Focusing of Hard X Rays by a Multilayer Laue Lens.” Phys. Rev. Lett. **96**, 127401, (2006).
29. H. Mimura *et al.*, “Efficient focusing hard X-rays to a size less than 30 nm by a total reflection mirror.” Appl. Phys. Lett. Submitted.